

The influence of gravitational lensing on the spectra of lensed QSOs

L.Č. Popović^{1,2*} and G. Chartas³

¹*Astronomical Observatory, Volgina 7, 11160 Belgrade 74, Serbia*

²*Astrophysikalisches Institut Potsdam, An der Sternwarte 16, 14482 Potsdam, Germany*

³*Astronomy and Astrophysics Department, Pennsylvania State University, University Park, PA 16802*

Accepted 2004 Received 2004 ; in original form 2004 July 8

ABSTRACT

We consider the influence of (milli/micro)lensing on the spectra of lensed QSOs. We propose a method for the observational detection of microlensing in the spectra of lensed QSOs and apply it to the spectra of the three lensed QSOs (PG 1115+080, QSO 1413+117 and QSO 0957+561) observed with Hubble Space Telescope (HST). We find that the flux ratio between images A1 and A2 of PG 1115+080 is wavelength-dependent and shows differential magnification between the emission lines and the continuum. We interpret this magnification as arising from millilensing. We also find that the temporal variations in the continuum of image C of QSO 1413+117 may be caused by microlensing, while the temporal variation observed in QSO 0957+561 was probably an intrinsic one.

Key words: Gravitational lensing – quasars: emission lines – quasars: Q0957+561, PG 1115+080, QSO 1413+117

1 INTRODUCTION

Gravitational macro and microlensing are well known phenomena that have been widely discussed in the literature (e.g., Schneider, Ehlers & Falco 1992; Zakharov 1997; Narayan & Betelmann 1999; Wambsganss 2001, Claeskens & Surdej 2002 and references therein). The influence of microlensing on the spectra (continuum and spectral lines) of lensed QSOs has been investigated mainly theoretically (Nemiroff 1988; Schneider & Wambsganss 1990; Wambsganss & Paczynski 1991; Popović et al. 2001a; Abajas 2002; Lewis & Ibata 2004). Some of the observational effects have also been presented in several papers (e.g., Lewis et al. 1998; Mediavilla et al. 1998; Wisotzki et al. 2003; Wucknitz et al. 2003; Chelouche 2003; Metcalf et al. 2004; Richards et al. 2004).

The influence of microlensing on the line profile of lensed QSOs was initially investigated by Nemiroff (1988) and Schneider & Wambsganss (1990). Recently Wandel et al. (1999) and Kaspi et al. (2000) using reverberation technique discovered that the broad line region (BLR) size was smaller than that assumed in the standard AGN model. Following this discovery, the influence of microlensing on the line profile of lensed QSOs in the UV/optical wavelength band, was revised and discussed in several papers (Popović 2001a; Abajas 2002; Lewis & Ibata 2004). Similar investigations have been performed in the X-ray spectral region

(Popović et al. 2001b; Chartas et al. 2002,2004; Popović et al. 2003; Dai 2003).

Abajas et al. (2002) noted that the influence of microlensing on the shapes of spectral lines can be very strong for high ionization lines arising from the inner part of the broad emission line region. The magnification depends on the size of the BLR and we therefore expect that distortions of spectral lines will not be observable in all microlensing events. Using the BLR size estimation for NGC 5548 (Peterson & Wandel 1999) and the relation between the radius of the BLR and optical luminosity, $R_{BLR} \sim L_{\lambda}^{-0.7}$ at $\lambda = 5100 \text{ \AA}$, given by Kaspi et al. (2000), Abajas et al. (2002) identified a group of 10 gravitational lensed systems in which microlensing of the BLR could be observed.

Observations and modeling of microlensing of the BLR are promising, because the study of the variations of the broad emission line shapes in a microlensed QSO image could constrain the size of the BLR and the continuum region (e.g., Lewis & Ibata 2004). Observations of microlensing of the profiles of Fe K α spectral lines in three multi-imaged QSOs were recently presented in Chartas et al. (2002,2004) and Dai et al. (2003). The observed variations of the Fe K α lines are in good agreement with theoretical predictions (Popović et al. 2001a; Popović et al. 2003). Observations of the effect of microlensing on the profile of broad UV emission lines (C IV and S IV/OIV) were recently reported by Richards et al. (2004).

The detection of microlensing from the distortion of

* E-mail: lpopovic@aob.bg.ac.yu; lpopovic@aip.de

the spectra of lensed QSOs is more complicated than inferring its presence from photometric observations. First of all, larger telescopes are needed to obtain the high signal-to-noise (S/N) ratio spectra, preferably with 2D spectrophotometry that can provide simultaneous spectra of all images. In addition, the intrinsic variability of lensed QSOs needs to be taken into account when comparing spectra of different images. Gravitational microlensing can also distort the spectrum of the continuum. Specifically, it is expected that microlensing is wavelength dependent (e.g., Wambsganss & Paczynski 1991; Lewis et al. 1988; Wisotzki et al. 2003) since the size of a continuum emission region of the accretion disk depends on the wavelength band.

According to the standard model of AGNs, a QSO consists of a black hole surrounded by a (X-ray and optical) continuum emitting region probably with an accretion disk geometry, a broad line region and a larger region that can be resolved in several nearby AGN that usually is referred to as the narrow line region (e.g., Krolik 1999).

Variability studies of QSOs indicate that the size of the X-ray emission region is of order 10^{14-16} cm (e.g., Chartas et al. 2001; Oshima et al. 2001, Dai et al 2003). An Fe K α fluorescence line detected in several AGN near 6.4 keV is thought to originate from within a few 10s of gravitational radii (e.g., Tanaka et al. 1995; Fabian et al. 1995). This line is thought to be a fluorescence line of Fe due to emission from a cold or ionized accretion disk that is illuminated from a source of hard X-rays originating near the central object. Aspects of this emission can provide a probe of strong gravity near a black hole.

Gravitational lensing is in general achromatic (the deflection angle of a light ray does not depend on its wavelength), however, the wavelength dependent geometry of the different emission regions may result in chromatic effects. Studies aimed at determining the influence of microlensing on the spectra of lensed QSOs need to account for the complex structure of the QSO central emitting region. Since the sizes of the emitting regions are wavelength dependent, microlensing by stars in the lens galaxy will lead to a wavelength dependent magnification. The geometries of the line and the continuum emission regions are in general different and there may be a variety of geometries depending on the type of AGN (i.e., spherical, disk-like, cylindrical, etc.).

On the other hand, in some cases the potential of the lens galaxy may be perturbed by small satellite galaxies or globular clusters (hereafter millilensing). These perturbations will add additional complexity to the magnification function.

To investigate the effects of microlensing, a method is needed that can be applied to the observed spectra. A technique that is often used (in cases where flux losses from slits are significant) relies on measuring the equivalent widths of spectral lines (Lewis et al. 1998; Wisotzki et al. 2003). One limitation of this approach is that it does not account for microlensing of the continuum component that may significantly affect the line equivalent widths.

The aim of this paper is to discuss the influence of gravitational (micro/milli)lensing on the spectra (continuum and spectral lines) of lensed QSOs. First in §2 we outline a model that includes the geometry of the line and continuum emission regions, as well as the magnification due to the lens galaxy and the stars in the lens galaxy. Based on this model

we propose a method for detecting microlensing events in the lines as well as in the continuum components of QSOs. In §3 we applied the method to a sample of lensed QSOs observed with HST, and in §4 we present our conclusions.

2 THE INFLUENCE OF LENSING ON QSO SPECTRA

We assume that the emitting region of a QSO is geometrically complex, and that the geometries and sizes of the continuum and the line emitting regions are different, i.e., that the unlensed surface brightness, $I(\lambda; X, Y)$ (in the case of X-ray $I(\lambda; X, Y) \rightarrow I(E; X, Y)$, where E is the emitted energy), can be written as a function of wavelength as,

$$I(\lambda; X, Y) = I^c(\lambda; X, Y) + I^L(\lambda; X, Y), \quad (1)$$

where $I^c(\lambda; X, Y)$ and $I^L(\lambda; X, Y)$ are the surface brightnesses of the continuum and the lines, respectively and X, Y are the coordinates of the emission region in the source plane. The magnification of the images depends in part on the projected mass distribution of the lens galaxy. We assume that the macro-magnification ($A(X, Y)$) is complex and can be represented as function of the X, Y coordinates in the source plane. Under these assumptions an observer will detect the following magnified intensity of an image (i),

$$\mathfrak{I}_i(\lambda; X, Y) = \mathfrak{I}_i^c(\lambda; X, Y) + \mathfrak{I}_i^L(\lambda; X, Y)$$

where

$$\mathfrak{I}_i^{c,L}(\lambda; X, Y) = I^{c,L}(\lambda; X, Y) \cdot A(X, Y) \quad (2)$$

In general one can expect an energy dependent magnification of the images of a lensed QSO resulting in different magnifications of the line and the continuum emission regions (as it was observed in the case of Q2237+0305, see Mediavilla et al. 1998).

Taking into account that the sizes of the continuum and the line emitting regions may be a function of wavelength, we write the fluxes as,

$$\Phi_i^{c,L}(\lambda) = \int_{\Sigma} I^{c,L}(\lambda; X, Y) \cdot A(X, Y) d\Sigma, \quad (3)$$

where Σ is the projection of the QSO emitting region in the source plane onto a plane perpendicular to the line-of-sight of the observer and $d\Sigma = dX dY$. As one can see from Eq. (3), in general, the fluxes, $\Phi_L^i(\lambda)$ and $\Phi_c^i(\lambda)$, depend on the geometry of the source as well as on the magnification caused by the lens galaxy.

If we assume there are no millilensing and the sizes of the emission regions are significantly smaller than the size of the macro-caustic, then we expect the magnification of the continuum and the line fluxes to be the same, i.e.,

$$\Phi_i^c(\lambda) = F^c(\lambda) \cdot A_i, \quad \Phi_i^L(\lambda) = F^L(\lambda) \cdot A_i. \quad (4)$$

where A_i is the macro-magnifications of the image i and $F^{c,L}(\lambda) = \int_{\Sigma} I^{c,L}(\lambda, X, Y) d\Sigma$.

The inference of a microlensing event (MLE) from the analysis of the spectral lines and the continuum spectral components of lensed QSOs can be complicated by several

effects that may include intrinsic variability of their fluxes and their spectra and the fact that intrinsic variability between different images of a lensed QSO will be time-delayed.

A possible solution to this problem is to obtain observations of all the images of a lensed QSO at different epochs, preferably with the time intervals between observations coinciding with the time-delays of the system. With such observations one can compare the flux of each component as a function of wavelength for different epochs, as well as the flux ratios between different images observed at a given epoch. We define the observed intensities of fluxes A and B as $\Phi_A(\lambda)$ and $\Phi_B(\lambda)$ at time t_0 and $\Phi'_A(\lambda)$ and $\Phi'_B(\lambda)$ at time t_1 , and the time-delay between the images as $\Delta t = t_1 - t_0$.

In principle, images of a lensed quasar are always being microlensed by stars in the foreground galaxy. This results in the continuous magnification as well as demagnification of the lensed quasar images. In the quiescent periods, when the magnification is low, the magnification map is smooth and one should not expect any detectable differences between the spectral energy distributions of images. In the case where magnification caustics are in the vicinity of the source the differential magnification of the continuum is expected to be significantly stronger and detectable (e.g., Wambsguss & Paczynski 1991). Consequently, hereafter we consider only high-magnification (A_{MLE}) microlensing events.

If a microlensing event (with a strong amplification) is present in only one of the images (e.g., A at time t_1), then the flux of this image will vary with time, and the magnified flux due to microlensing can be written as:

$$\Phi'_i(\lambda) = \int_{\Sigma} \mathfrak{S}_i(\lambda; X, Y) \cdot A_{MLE}(X, Y) d\Sigma = A_i \int_{\Sigma} [I^c(\lambda; X, Y) + I^L(\lambda; X, Y)] \cdot A_{MLE}(X, Y) d\Sigma \quad (5)$$

where Σ is the projected surface of the macrolensed image at the source distances and A_{MLE} is the amplification due to microlensing. The flux ratio ($R_{A',A} = \Phi'_A(\lambda)/\Phi_A(\lambda)$) of the same image at two different epochs separated by the time-delay is:

$$R_{A',A} = \frac{\int_{\Sigma} [I^c(\lambda; X, Y) + I^L(\lambda; X, Y)] A_{MLE}(X, Y) d\Sigma}{[F^c(\lambda) + F^L(\lambda)]}, \quad (6)$$

and the flux ratio between different images observed at the same epoch is

$$R_{A',B'} = \frac{A_1}{A_2} \frac{\int_{\Sigma} [I^c(\lambda; X, Y) + I^L(\lambda; X, Y)] A_{MLE}(X, Y) d\Sigma}{[F^c(\lambda) + F^L(\lambda)]}. \quad (7)$$

We define as an indicator of variability (σ):

$$\sigma(\lambda) = R_{A',A} - R_{B',B}. \quad (8)$$

In general $\sigma = 0$ indicates no variability. We note the rare case where $\sigma = 0$ and variability is present. This condition can occur when the fluxes of both images A and B change by the same factor between epochs t_0 and t_1 . The probability of such an event is negligible. If $\sigma \neq 0$, then we investigate the source of the variability.

If microlensing of only one image (e.g. A) is present and there is no other source of variability, then the average magnification caused by microlensing is,

$$\overline{A}_{MLE}(\lambda) = \frac{\int_{\Sigma} [I^c(\lambda; X, Y) + I^L(\lambda; X, Y)] A_{MLE}(X, Y) d\Sigma}{[F^c(\lambda) + F^L(\lambda)]}.$$

From Eqs. (5-7) we write the average magnification caused by microlensing as

$$\overline{A}_{MLE}(\lambda) = \frac{\Phi'_A(\lambda)}{\Phi_A(\lambda)} = \frac{A_2}{A_1} \cdot \frac{\Phi'_A(\lambda)}{\Phi'_B(\lambda)}, \quad (9)$$

where A_1 and A_2 are the macro-magnifications of images A and B, respectively.

Eq. (9) is only valid for the case where microlensing is occurring in one component. For the case where intrinsic variability (σ_I) is present we have

$$\sigma_I = R_{A',A} - \frac{A_2}{A_1} R_{A',B'} \neq 0, \quad (10)$$

Also, σ_I will be different from zero if both images are microlensed at the same time. This may be checked by comparing the spectra of two images observed at two different epochs separated by the time-delay. If the relation

$$R_{A'B} = \frac{\Phi_{A'}}{\Phi_B} = \frac{A_1}{A_2},$$

holds we conclude that intrinsic variation is present, otherwise if it is not satisfied we conclude that both images are microlensed.

On the other hand, taking into account that the total flux is the sum of line and continuum fluxes (see Eq. (1)), the average magnification of only the line is

$$\begin{aligned} \overline{A}_{MLE}^L(\lambda) &= \frac{\Phi_{A'}^L(\lambda) - \Phi_{A'}^c(\lambda)}{\Phi_A^L(\lambda) - \Phi_A^c(\lambda)} = \\ &= \frac{A_2}{A_1} \frac{\Phi_{A'}^L(\lambda) - \Phi_{A'}^c(\lambda)}{\Phi_{B'}^L(\lambda) - \Phi_{B'}^c(\lambda)}, \end{aligned} \quad (11)$$

and in the case of millilensing one can expect that magnifications in the line and in the continuum are different ($A^L \neq A^c$) as well as that these magnifications are wavelength dependent.

In Table 1 we point out several cases where our method can be used. There are more complex cases not listed in Table 1 such as the combination of milli and microlensing, microlensing and intrinsic variability and microlensing of both images. Observations in several epochs separated by the time-delay are useful in distinguishing between these complex cases.

3 OBSERVATIONS: SEVERAL EXAMPLES, RESULTS AND DISCUSSION

Our method of analyzing the spectra of lensed quasars outlined in §2 can be applied accurately when simultaneous observations of spectra of images of a lensed QSO at two different epochs separated by the time-delay are available. In many cases the time-delay of a system is unknown. In such a situation our method can still be applied to estimate

Table 1. A list of cases where our proposed method can be used to infer the presence of millilensing, microlensing and intrinsic variability.

The case	Description
I) $\sigma = 0$ and $R_{AB} = R_{A'B'} = \text{const.}$	No variability or millilensing present
IIa) $\sigma = 0$, $R_{AB} = R_{A'B'} = f(\lambda)$ and/or $A^L \neq A^c$ IIb) $\sigma = 0$, $R_{AB} = R_{A'B'} = \text{const.}$ and $A^L \neq A^c$	There is no variability, but millilensing or differential extinction might be present (see e.g., Wucknitz et al. 2003), if $R_{AB} = f(\lambda)$ cannot be explained by extinction \rightarrow millilensing is present
III) $\sigma \neq 0$, $\sigma_I \neq 0$, and $R_{A'B} = \frac{A_1}{A_2}$	Intrinsic variability is present
IVa) $\sigma \neq 0$, $\sigma_I = 0$, $R_{A,B} \neq f(\lambda)$ and $R_{A',B'} = f(\lambda)$	Microlensing of one image at time t_1
IVb) $\sigma \neq 0$, $\sigma_I = 0$, $R_{A,B} = f_1(\lambda)$, $R_{A',B'} = f_2(\lambda)$ and $R_{A'A} = 1$ (or $R_{B'B} = 1$)	Microlensing of one image at times t_0 and t_1 (timescale of microlensing is longer than time delay)

the origin of the magnification. We note that the application of our method is limited by the S/N of the component spectra, e.g., in the case of low S/N, non zero values for the variability indicator sigma and chromatic effects may only be detected in cases where there are large flux magnifications caused by microlensing or other effects listed in Table 1. Therefore high S/N spectra are needed to apply our model accurately.

Here we apply our method to several observations of lensed quasars performed with HST. By inspection of the HST database we found only three lensed quasars with simultaneous observations of all images at different epochs: QSOs Q0957+561, PG 1115+080 and Q1413+117. In this section we compare the spectra between different images as well as between the same image at different epochs using the method described above. The STARLINK DIPSO software package (Howarth et al. 2003) was used to analyze the spectra.

3.1 Q0957+561

Images A and B of Q0957+561 have been observed with HST at several epochs. In the HST archive we found observations of both images made with the FOS G270 and obtained in 1995 (Jan 26, Oct 20, Nov 04, Nov 17, and Dec 14) that we used for our analysis. We also found observations of only image A of Q0957+561 with STIS performed on 1999 April 04, and observations of only image B on 2000 June 2, and only image A on 2000 September 8, but these observations have not been used in our present analysis. A detailed description of all observations and the analysis of the spectra can be found in Michalitsianos et al. (1997), Dolan et al. (2000) and Hutchings (2003).

A first inspection shows that images A and B have similar spectra (practically the same), with the exception of the spectra observed on 1995 January 26 (see Figure 1). We applied the method described above to all observed spectra of Q0957+561 obtained in 1995, comparing the spectra of images A and B from different epochs. From observations taken within the period October–December we did not detect any significant difference between the spectra that would indicate a microlensing event or intrinsic variability. A slight but not statistically significant difference exists in the variability indicator σ (see Figures 2a, 3a and 5a). A significant differ-

ence between images was only detected in spectra observed on 1995 January 26, (Figures 2b, 3b and 5b). In Figure 2 we present the variability indicator between observations performed on October 20 and December 14, 1995 (Fig. 2a) as an example. The variability indicator σ (similar to the case of all spectra observed within the period October–December), does not significantly differ from zero and taking into account the noise in the spectra we conclude that significant variability is not present in this time interval. On the other hand a comparison between the spectra observed on 1995 January 26 and spectra taken at other epochs shows significant differences. As an example the variability indicator σ between observations performed on Jan 26 and Dec 14, 1995 is shown in Figure 2b. Variability is clearly present in the continuum as well as in the Ly α line (the location of the line is indicated with a dashed line). To investigate the nature of this variability we determined the flux ratio using Eq. 6. As shown in Figure 3, the flux ratio for the observed spectra in the period October–December is practically one, whereas the flux ratio of the spectra observed on 1995 January 26, is ~ 1.8 times higher than the ratio observed during the period October–December.

We do not find any significant wavelength-dependence of the variability indicator σ , the flux ratio $R_{A,A'}$ between the same image at different epochs or the flux ratio $R_{A,B}$ between different images for the same epoch.

Moreover, in Figure 4 we show that at three different epochs within the October–December period the flux ratio $R_{A,B}$ is consistent with the magnification resulting from macrolensing. Using the optical magnitudes of images A and B of Q0957+561 available from the *Castles* database¹ we obtained a flux ratio of $F_A \approx 1.08 F_B$. A comparison of the flux ratios of Figure 4 also shows that on 1995 January 26, the flux of the continuum of image B was significantly larger than that of image A.

We use Eq. (10)² to investigate the nature of the variability in Q0957+561. As shown in Figure 5, the variability ($\sigma_I \neq 0$) seen on January 26, 1995 is most likely intrinsic.

Here we briefly discuss the absorption line detected

¹ <http://cfa-www.harvard.edu/castles/>

² Here we approximate the amplification ratio as $\frac{A_2}{A_1} = \frac{A_B}{A_A} \approx R_{B,A}$

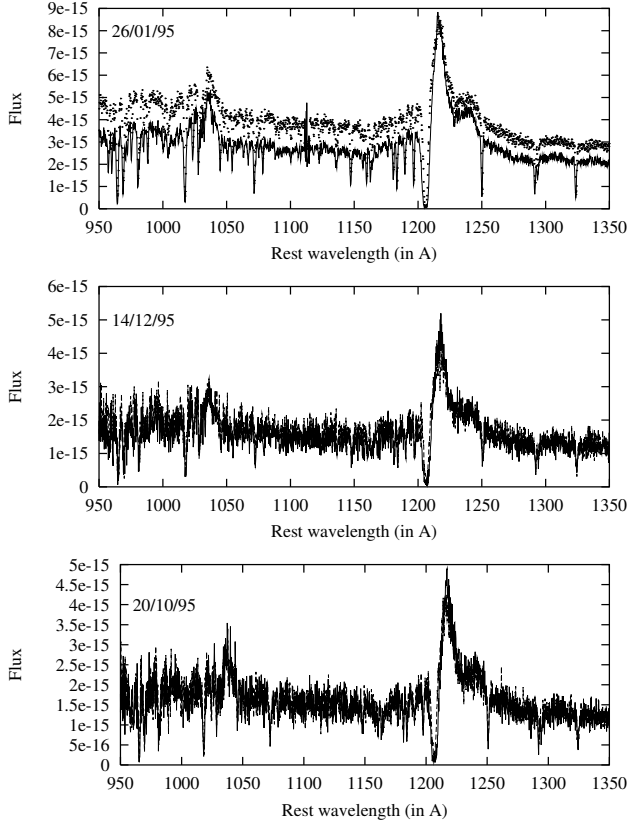


Figure 1. The spectra of Q0957+561 observed with HST for three different epochs. The solid line and dots indicate the spectra of images A and B, respectively. The flux is given in $\text{erg cm}^{-2}\text{sec}^{-1}\text{Å}^{-1}$.

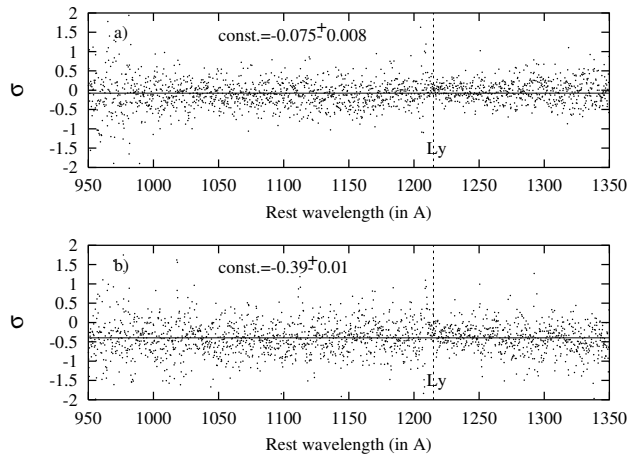


Figure 2. The variability indicator $\sigma = (I'_A/I_A) - (I'_B/I_B)$ calculated for the spectra of Q0957+561 for the epochs: a) 1995 December 14 and 1995 October 20 (case I); b) 1995 January 26 and 1995 December 14 (case II). The vertical dashed line indicates the location of the Ly α line.

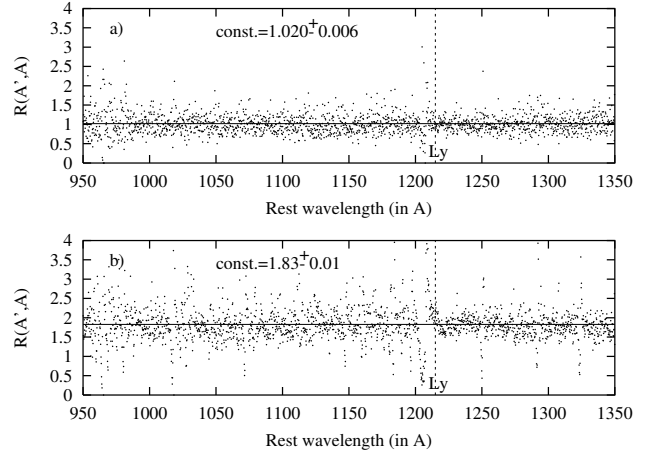


Figure 3. The flux ratio between the spectra of image A of Q0957+561 for the epochs: a) 1995 December 14 and 1995 October 20 (case I); b) 1995 January 26 and 1995 December 14 (case II).

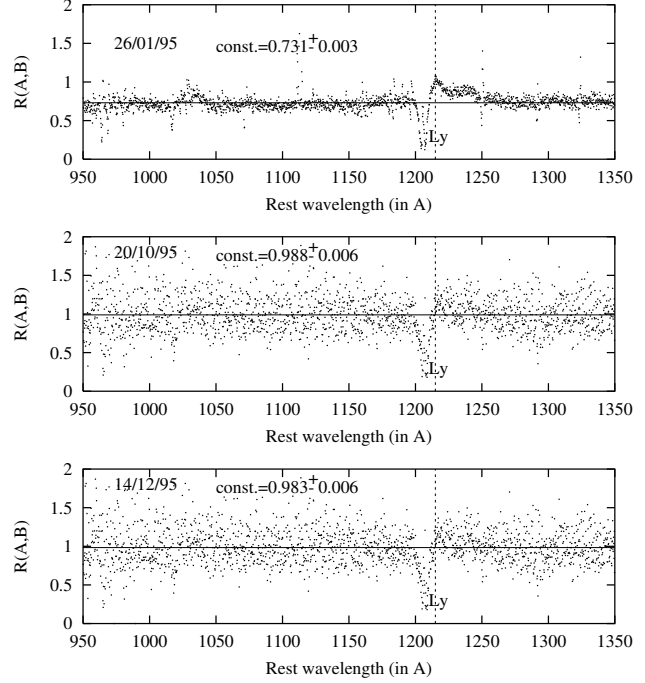


Figure 4. The flux ratio between images A and B of Q0957+561 observed for the listed epochs.

blue-wards of Ly α originating from a damped Lyman alpha (DLA) system at a redshift of ~ 1.391 (Michalitsianos 1997). A comparison of the flux ratios between images at all epochs indicates that the absorption line is stronger in image A than in image B (see Figure 4). This is in agreement with the previous analysis reported by Michalitsianos et al. (1997). Such differences in the absorption between images indicates inhomogeneity in the DLA system that may arise from the different paths of the rays of the two images (see e.g. Chelouche 2003).

To summarize, our analysis of the spectra of Q0957+561 taken in January, October and December of 1995 indicates

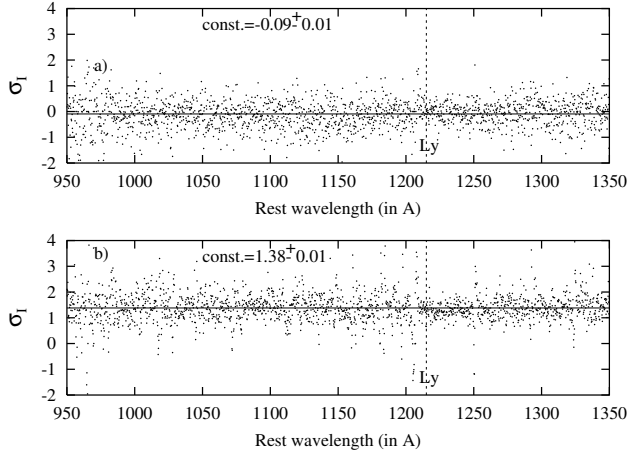


Figure 5. σ_I , an indicator of intrinsic variability of Q0957+561 spectra is shown for the epochs: a) October and December 1995 and b) January and December 1995.

that: i) the strong magnification detected in the continuum and in the Ly α line is most likely caused by intrinsic variability of the QSO, ii) during this variation image A has a stronger line flux than image B and image B has a stronger continuum flux than image A, iii) the flux ratio of the continuum is not wavelength-dependent.

3.2 PG 1115+080

PG 1115+080 is a lensed QSO with a redshift of 1.72. The time-delay between images B and C of 23 ± 3.4 days was initially measured by Schechter et al. (1997) whereas a later analysis by Barkana (1997) resulted in a value of 25 ± 2 days. For the purpose of applying our method we ignore the time-delay between images A1 and A2. Impey et al. (1998) had reported an anomalous flux ratio between images A2 and A1. Their observations ruled-out differential extinction and microlensing as explanations for the anomalous flux ratio, because of a lack of variability. They conclude that since an expected flux ratio between images A2 and A1 of ~ 1 is a generic feature of the large-scale potential near a fold caustic (from a simple lens model), only a potential perturbation intermediate between that produced by stars in the lens galaxy (microlensing) and by the overall galaxy can explain the anomalous flux ratio, and that the potential of PG 1115+080 must be perturbed either by a satellite galaxy or a globular cluster, i.e. that millilensing is present.

Our search of the HST database found an observation of PG 1115+080 made on 1995 June 07, which covers the wavelength range from 850 Å to 1200 Å (rest wavelength) and observations made on 1996 January 21 (image A1) and on 1996 January 24 (image A2) that cover the wavelength range from 850 to 1750 Å (rest wavelength). These observations were performed with the G270H and G400H gratings. More details describing these observations can be found in Bechtold et al. (2002).

First, we calculated the indicator of variability (σ) and intrinsic variability (σ_I) between observations made on 1996 January 21 (image A1) and on 1996 January 24 (image A2) for the wavelength range 850 Å – 1200 Å. As shown in Figure 6a, the variability indicator is not significant, but it appears

that a low level of variability may be present ($\sigma \approx 0.1$). In Figure 6b we show that weak intrinsic variability may be present ($\sigma_I \approx 0.05$). However, both indicators of variability are negligible with respect to the level of the rms noise (~ 0.3).

To further investigate the significance of variability, we determined the flux ratios between the same images at two epochs. As shown in Figure 7, variability is not significant. Specifically the continuum flux of image A1 increased by about 3%, and that of image A2 decreased by about 7% between July 1995 and January 1996. (see Figure 7), however, both variations are insignificant relative to the level of the rms noise.

We have also calculated the flux ratios between images A1 and A2 for the July 1995 and January 1996 observations (see Figures 8). As shown in Figure 8 the flux ratios tend to be slightly different for different epochs, not only in magnitude, but also in the shape of the wavelength dependence. This result should be taken with caution because of the high level of noise, especially in the spectra obtained on 1996 January. We also find that the emission lines in the spectrum of image A2 were stronger than those in image A1 during the July 1995 and January 1996 observations. This difference in line strength is more obvious in the flux ratio between images A1 and A2 of PG 1115+080 for the observation made on 1996 January when plotted in the spectral range of 850 Å – 1750 Å (see Figure 9). The N III λ 990.98, O IV λ 1033.82, Ly α , Si IV λ 1396.76 and C IV λ 1549 lines are stronger in image A2 than in image A1. We note that the flux ratio as defined in Eqs. (6) – (7) includes both line and continuum components. Consequently, the difference of the intensity of the emission lines in images A1 and A2 of PG 1115+080 as shown in Figures 8 and 9 may arise in part from the different magnifications of the underlying continua in images A1 and A2.

We assumed that the relative macro-magnification of images A1 and A2 is achromatic (i.e., case II, Table 1). To search for possible differences between the magnification of the spectral lines and continuum, we scaled the spectra observed in January 1996 of both images on the same continuum level. In Figure 10a we compare the flux vs. wavelength of images A1 and A2 of PG 1115+080 after scaling the continuum of image A2 to that of A1 (multiplying the flux of the image A2 continuum by the function $R(A1, A2) = 2.75 - 5.9 \cdot 10^{-4} \cdot \lambda$). We notice that the spectrum of image A2 has stronger lines (with respect to the local continuum) than those of image A1. This is expected if we have microlensing or millilensing of the continuum. But this difference cannot be explained by microlensing since the indicator of variability is small with respect to rms noise ($\sigma \approx 0.1$). The difference between the continuum and line amplifications is more likely the result of millilensing. Here we should mention that long-term microlensing may produce a similar effect (case IVb), even with the indicator of variability being negligible in this case, we cannot completely exclude long-term microlensing.

If we assume that the indicator of variability is negligible ($\sigma \sim 0$) and millilensing is present (case (2) of §2.1), then we expect millilensing to cause different magnifications of the continuum and the emission line components, as indicated in Eq. (3). Since the line and continuum emission com-

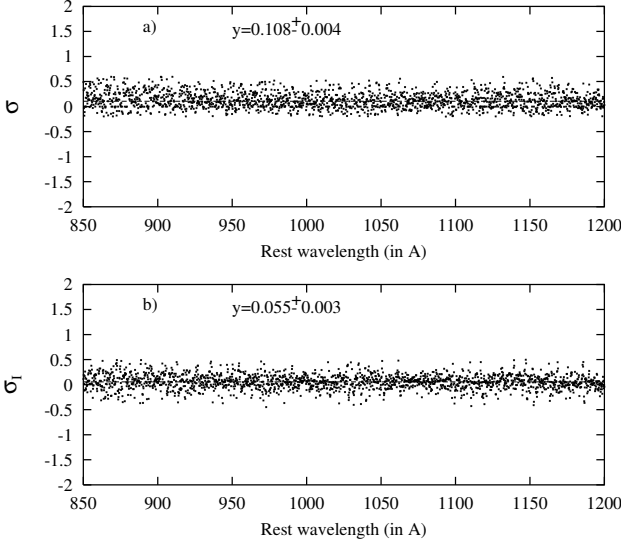


Figure 6. a) The variability indicator (σ) and b) intrinsic variability indicator (σ_I) between images A1 and A2 of PG 1115+080

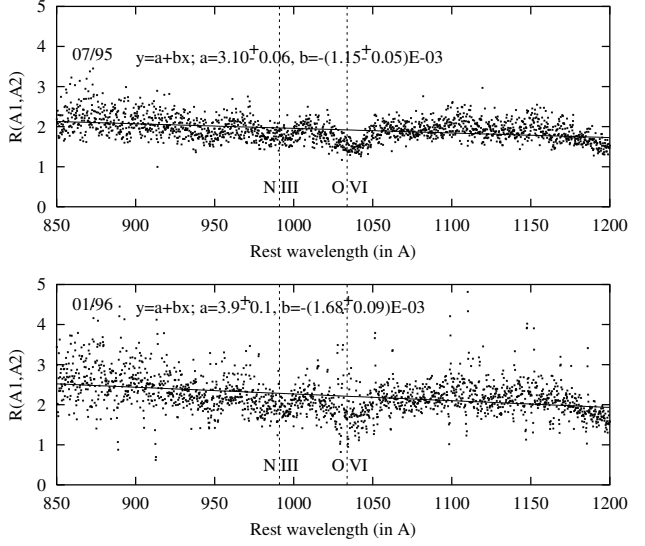


Figure 8. The flux ratio as a function of wavelength between images A1 and A2 of PG 1115+080 for two different epochs

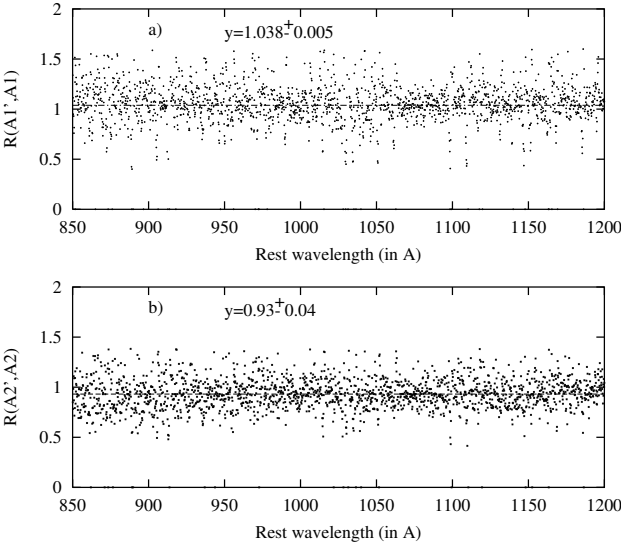


Figure 7. The flux ratio between epochs 1995 July and 1996 January for a) image A1, and b) image A2.

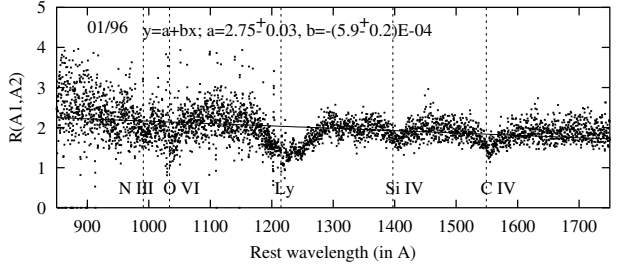


Figure 9. The flux ratio of images A1 and A2 of PG 1115+080 in the wavelength band of 850 – 1750 Å

ponents are additive (Eqs. 1-3), we subtracted the continuum in both images (Eq. 11) and compared the line fluxes.

A comparison of the line fluxes in the spectra of images A1 and A2 with subtracted continua is shown in Figure 10b. A small differences in these fluxes can be due to uncertainties in the subtracted continua, but we can conclude that the A1/A2 flux ratio of the lines is $(A1/A2)_L \sim 1$. This ratio corresponds to the expected value of ~ 1 if no micro or millilensing were present because the images are symmetrically arranged near a fold caustic (see Schneider et al. 1992). On the other hand, the ratio of A1/A2 continuum flux is wavelength dependent and in the observed wavelength range (from 850 Å to 1750 Å) can be approximated by the function $R(A1, A2)_{\text{continuum}} \approx 2.75 - 5.9 \cdot 10^{-4} \cdot \lambda$, i.e. the amplification

in the continuum is changing from $(A1/A2)_{\text{continuum}} \approx 2.3$ at 850 Å to $(A1/A2)_{\text{continuum}} \approx 1.75$ at 1750 Å.

Since millilensing is similar to microlensing, we may expect the line profiles of images A1 and A2 to be different (Popović et al. 2001, Abajas et al. 2002). In Figure 11 we compare the Ly α and C IV λ 1549 line profiles between images A1 and A2. We also show a comparison between the Ly α and C IV λ 1549 line profiles from the spectrum of image A2 since the line emitting regions of different emission lines may be different (e.g., Wandel et al. 2000; Kaspi et al. 2000).

For the purpose of these comparisons, we normalized the fluxes of the Ly α and C IV λ 1549 lines to one and converted wavelengths to velocities: $\lambda \rightarrow X = (\lambda - \lambda_0)/\lambda_0$. As shown in Figure 11 there are no significant differences between the line profiles of the same lines in the spectra of images A1 and A2. These comparisons suggest that millilensing does not affect the emission line region of PG 1115+080.

In Figure 11c, we note that the red wing of the Ly α line is stronger than the C IV red wing. We propose that this difference is likely caused by the contribution of the NV λ 1240 line. We note that such a strong NV λ 1240 doublet ($F_{NV} \sim 0.5 F_{Ly}$) is unusual for QSOs, with a more typical value expected to lie in the range $F_{NV} \sim (0.1 - 0.2) F_{Ly}$ (e.g., Laor 1994).

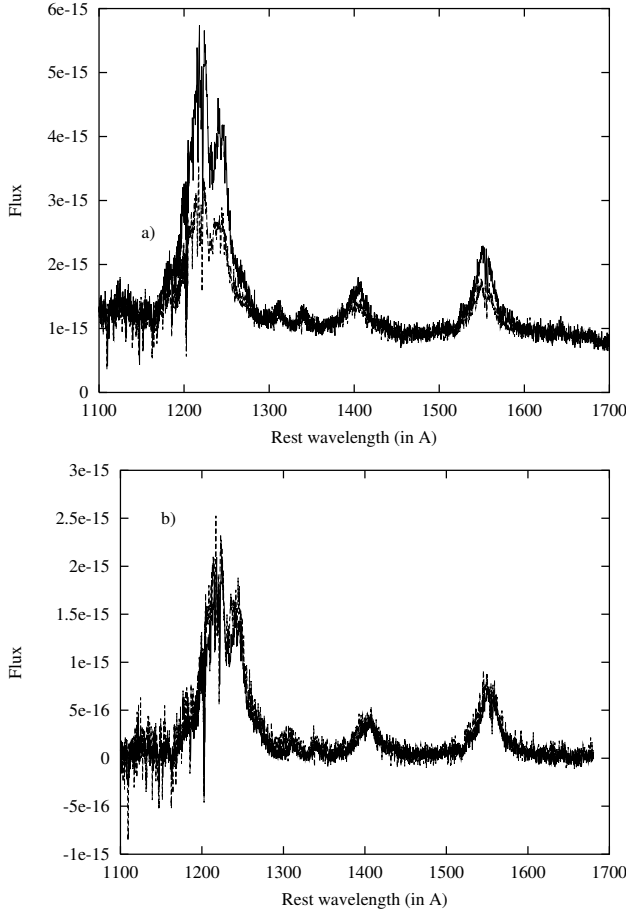


Figure 10. The flux (given in $\text{erg cm}^{-2}\text{sec}^{-1}\text{Å}^{-1}$ units) of image A1 of PG 1115+080 (dashed line) compared to that of image A2 of PG 1115+080 (solid line): a) after scaling the spectra of both images to the same continuum (the continuum level of image A1), and b) after subtraction of the continuum in both images.

Our investigation of the spectra of images A1 and A2 of PG 1115+080, confirms the anomalous spectral distribution and relative magnifications of these two images, first noted by Impey et al. (1998). The main results of our analysis of the spectra of PG1115+080 are as follows: i) We only detect very weak variability in images A1 and A2 of PG 1115+080 between two observations; ii) the differential magnification of the line and the continuum components as well as wavelength-dependent amplification may be caused by millilensing. This is consistent with an earlier proposal by Impey et al. (1998) that suggested the presence of significant perturbations to the main lens galaxy of the PG 1115+080 lens system by a satellite galaxy or globular cluster. iii) Millilensing affects the continua of A1 and A2 in observed wavelength range ($F(A1)_C/F(A2)_C \approx 1.75 - 2.3$, expected ~ 1), but it does not appear to significantly affect the line profiles of the images ($F(A1)_L/F(A2)_L \approx 1$).

3.3 QSO 1413+117 - Cloverleaf

The spectra of the images of QSO 1413+117 were observed in the spectral ranges of 900–1350 Å and 1300–1800 Å and an analysis of these spectra was presented in Monier et al.

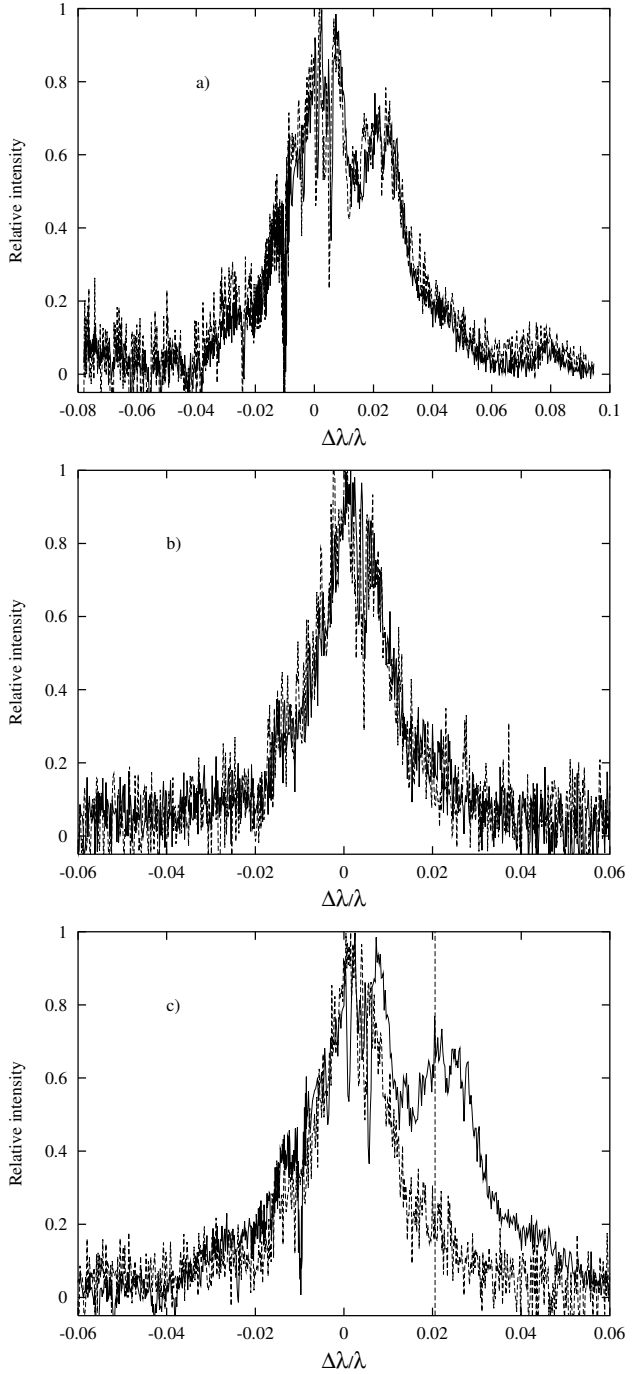


Figure 11. A comparison between : a) the $\text{Ly}\alpha$ line profiles of images A1 and A2 of PG 1115+080; b) the C IV line profiles of images A1 and A2 of PG 1115+080; c) the $\text{Ly}\alpha$ and C IV line profiles of image A2 of PG 1115+080 (the vertical dashed line shows the position of the N v $\lambda 1240$ line).

(1998). They found that the emission spectral lines show an intrinsic absorption component and that the emission lines in the spectrum of image D are significantly weaker than in the other three images.

For our analysis we used the observations performed on 1993 June 23, (images A and D) and 1993 June 27, (images B and C) covering the spectral range 1300 – 1800 Å and

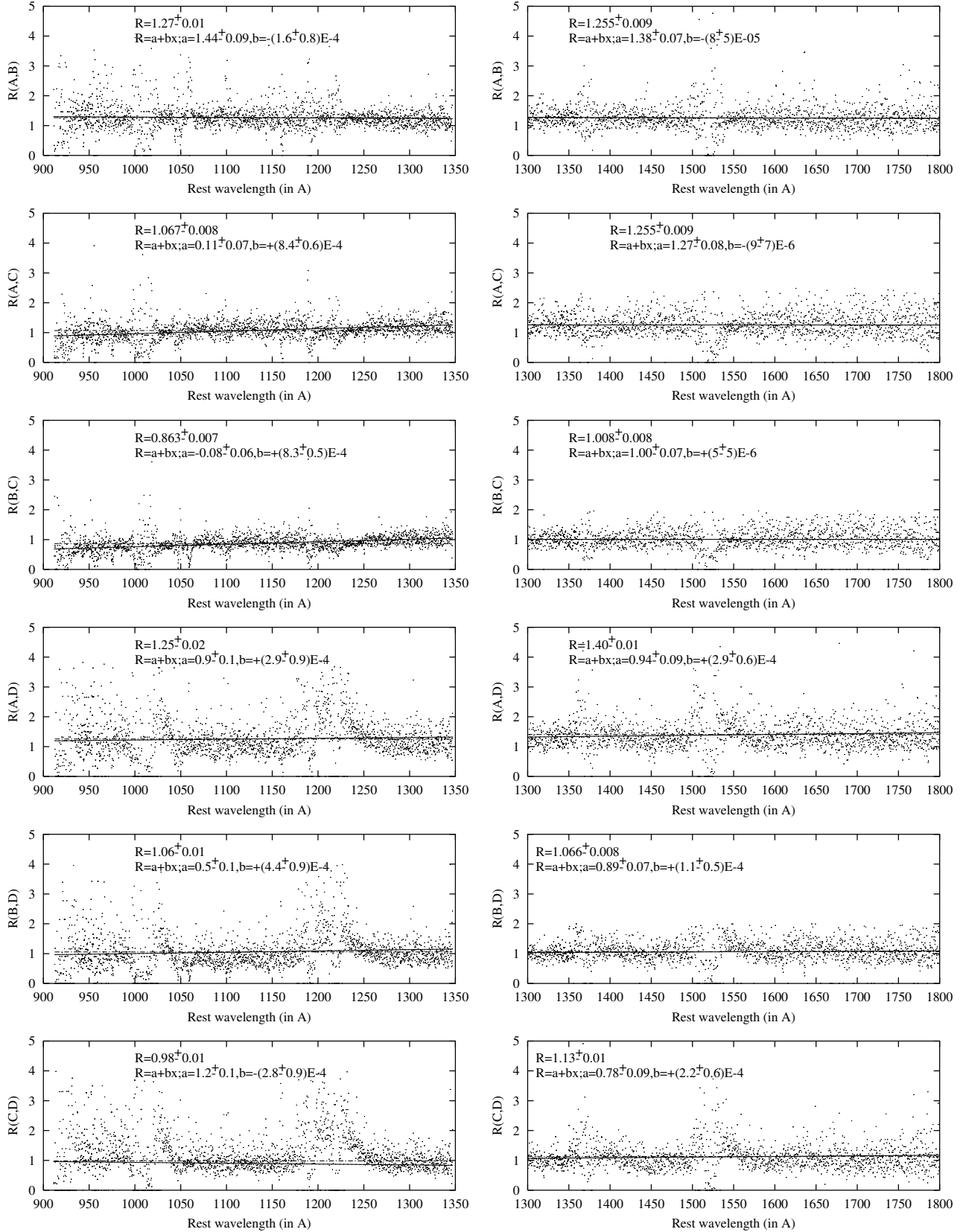


Figure 12. The flux ratio ($R_{i,j}$) of different images of QSO 1413+117 observed on the same date. Left panels: $R_{i,j}$ versus wavelength ranging from 900 Å to 1350 Å. Observations were made on 1994 December 24. Right panels: $R_{i,j}$ versus wavelength ranging from 1300 Å to 1800 Å. Observations of images A and D were performed on 1993 June 23 and of images B and C on 1993 June 27. From top to bottom, we show the flux ratios between the following images: A and B, A and C, B and C, A and D, B and D; C and D. The solid and dashed lines indicate the best fits of $R_{i,j} = a + b \cdot \lambda$ and $R_{i,j} = \text{const}$, respectively.

December 24, 1994 (all images) covering the spectral range 900 – 1350Å. The number and separation in time of these observations are not ideal for an accurate application of our method, however, as we will show we can still use our method to discuss the presence of a lensing event.

In Figure 12 we show the flux ratios as a function of wavelength (for both spectral ranges) of all images of QSO 1413+117. We fit the flux ratios with models of the form $R = a + b \cdot \lambda$ and $R = \text{const}$.

An inspection of the flux ratios indicates that:

i) during the first epoch (1994 December 24) only the ratios $R(A, C)$ and $R(B, C)$ have a significant non-zero slope, i.e., they are wavelength-dependent. This might also be the case for $R(C, D)$, but due to large residuals in the emission lines and the high level of noise of the ratio this result should be taken with caution. In the other cases the ratios tend to be constant.

ii) the flux ratios $R(A, B)$, $R(A, D)$, and $R(B, D)$ show no significant differences between all epochs observed, but flux ratios containing image C are different between epochs, i.e., $R(C, D)$, $R(B, C)$, and $R(A, C)$ show significant changes of the fitted slope between epochs.

iii) the spectra of image D for all observations show weaker UV emission lines than those of the remaining images as was previously noted in Monier et al. (1998).

From these observations we conclude that significant variability only of image C is present, and considering that the ratios $R(A, C)$ and $R(B, C)$ tend to be wavelength-dependent, we suspect that microlensing of image C was likely present during the observations.

4 CONCLUSIONS

In this paper we investigated the influence of gravitational lensing on the spectra of lensed QSOs. Starting from the assumption that the magnification due to a lens is in general a complex function, (i.e., the presence of globular clusters or satellite dwarf galaxies in the lens galaxy may introduce perturbations to the potential of the principal lens galaxy as noted by Impey et al. 1998) and that the line and continuum emitting regions are different in sizes and in geometries, we found that the magnification of the spectra of the different images may be chromatic (as was noted in Wambsganss & Paczyński 1991; Lewis et al. 1998; Wisotzki et al. 2003 and Wucknitz et al. 2003).

Here we briefly summarize several conclusions that arise from Eqs. (1-11) in §2:

i) in general the complex geometries of the emitting regions of QSOs and the complex potentials of the lens galaxies need to be taken into account when determining their influence on the observed spectra of the continuum and line emission;

ii) microlensing events lead to wavelength-dependent magnifications of the continuum that can be used as indicators of their presence;

iii) the average magnification due to microlensing may be determined from the flux ratio of an image observed at two different epochs separated by the time-delay and from the flux ratio between different images observed at the same time;

Here we propose a method to infer the presence of mi-

cro-lensing, millilensing and intrinsic variability in one or both of the images of a lensed quasar. The method is outlined in the following steps:

(a) Obtain simultaneous observations of the spectra of the images of a lensed quasar (at least) at two different epochs separated by the time-delay.

(b) Calculate the variability parameters σ and σ_I using equations (8) and (10), and determine the flux ratios $R_{A'A}$, $R_{B'B}$, R_{AB} , $R_{A'B'}$, and $R_{A'B}$.

(c) Use Table 1 to determine the possible presence of microlensing, millilensing or intrinsic variability of the quasar.

Using our proposed method we investigated the influence of microlensing on the FOS spectra of three lensed QSOs. We presented an example of the chromatic effect in our analysis of the FOS spectra of PG 1115+080. In particular, the application of our lensing method to this system indicates that the line and continuum components of the lensed QSO spectra of PG1115+080 have different magnifications during the HST observations.

The application of our method to investigate the effect of lensing on the spectra of lensed QSOs may be useful not only for constraining the unresolved structure of the central regions of QSOs, but also for providing insight to the complex structure of the lens galaxy and possible substructure in the lens galaxy.

ACKNOWLEDGMENTS

This work is a part of the project "Astrophysical Spectroscopy of Extragalactic Objects" supported by the Ministry of Science and Technologies and Development of Serbia and the Alexander von Humboldt foundation through the program for foreign scholars. We would like to thank the anonymous referee for very useful comments.

REFERENCES

- Abajas, C., Mediavilla, E.G., Muñoz, J.A., Popović, L. Č., & Oscoz A. 2002, ApJ 576, 640.
- Barkana, R. 1997, Apj, 489, 21
- Bechtold, J., Dobrzycki, A., Wilden, B., Morita, M., Scott, J., Dobrzycka, D., Tran, K.-V., Aldcroft, T. L. 2002, ApJS, 140, 143.
- Chartas, G., Dai, X., Gallagher, S. C., Garmire, G. P., Bautz, M. W., Schechter, P. L., & Morgan, N.D. 2001, ApJ, 558, 119
- Chartas, G., Agol, E., Eracleous, M., Garmire, G., Bautz, M. W., Morgan, N. D. 2002, ApJ, 568, 509
- Chartas, G., Eracleous, M., Agol, E., Gallagher, S.C. 2004, ApJ, 606, 78.
- Chelouche, D. 2003, ApJL, 43.
- Claeskens, J.-F., Surdej, J. 2002, AARv 10, 263.
- Dai, X., Chartas, G., Agol, E., Bautz, M. W., & Garmire, G.P. 2003, ApJ, 589, 100
- Dolan, J. F., Michalitsianos, A. G., Nguyen, Q. T., Hill, R. J. 2000, ApJ, 539, 111
- Fabian, A. C., Nandra, K., Reynolds, C. S., Brandt, W. N., Otani, C., Tanaka, Y., Inoue, H., Iwasawa, K., 1995, MNRAS, 277L, 11

- Howarth, I.D., Murray J., Mills, D., Berry, D.S. 2003, Starlink User Note, No. 50.24 (www.starlink.rl.ac.uk/star/docs/sun50.htx/sun50.html)
- Hutchings, J. B. 2003, AJ, 126, 24
- Impey, C. D., Falco, E. E., Kochanek, C. S., Lehr, J., McLeod, B. A., Rix, H.-W., Peng, C. Y., Keeton, C. R. 1998, ApJ, 509, 551
- Kaspi, S. Smith, P. S., Netzer, H., Maoz, D., Jannuzi, B. T., Givon, U. 2000 ApJ, 533, 631
- Krolik, J. H. 1999, 'Active galactic nuclei : from the central black hole to the galactic environment' Princeton, N. J. : Princeton University Press,
- Laor, A., Bahcall, J. N., Jannuzi, B. T., Schneider, D. P., Green, R. F., Hartig, G. F. 1994, ApJ, 420, 110.
- Lewis, G. F., Ibata, R.A. 2004, MNRAS, 348, 24L (astro-ph/0310818)
- Lewis, G. F., Irwin, M. J., Hewett, P. C., Foltz, C. B. 1998, MNRAS, 295, 573.
- Mediavilla, E., Arribas, S., del Burgo, C., Oscoz, A., Serradricart, M., Alcalde, D., Falco, E. E., Goicoechea, L. J., Garcia-Lorenzo, B., Buitrago, J. 1998, ApJ, 503, L27.
- Metcalf, R. B., Moustakas, L. A., Bunker, A. J., Parry, I. R. 2004, ApJ, 607, 43
- Michalitsianos, A. G., Dolan, J. F., Kazanas, D., Bruhweiler, F. C., Boyd, P. T., Hill, R. J., Nelson, M. J., Percival, J. W., van Citters, G. W. 1997, ApJ, 474, 598.
- Monier, E. M., Turnshek, D. A., Lupie, O. L. 1998, ApJ, 496, 177
- Narayan R., Bartelmann M. : 1999, Formation of Structure in the Universe (Eds. A. Dekler, J.P. Ostriker), Cambridge University Press, 360.
- Nemiroff, R.J., 1988, ApJ 335, 593.
- Oshima, T., Mitsuda, K., Ota, N., Yonehara, A., Hattori, M., Mihara, T., Sekimoto, Y. 2001, 551, 929
- Peterson, B. M., Wandel, A. 1999, ApJ, 521, 95
- Popović, L.Č., Jovanović, P., Mediavilla, E.G., Zakharov, A.F., Muñoz J., Abajas, C. 2004, in preparation.
- Popović, L.Č., Mediavilla, E.G., & Muñoz J., 2001a, A&A 378, 295.
- Popović, L., Č., Mediavilla, E.G., Muñoz J., Dimitrijević, M.S., & Jovanović, P. 2001b, Serb. Aston. J., 164, 73.
- Popović, L.Č., Mediavilla, E.G., Jovanović, P., & Muñoz, J.A., 2003, A & A, 398, 975
- Richards, G.T., Keeton, R.C., Bartosz, P. et al. 2004, ApJ, 610, 679.
- Schechter, P. L., Bailyn, C. D., Barr, R. et al. 1997, ApJ, 475, L85
- Schneider, P., Ehlers, J., Falco, E. E. 1992, Gravitational Lenses, Springer-Verlag Berlin Heidelberg New York.
- Schneider, P. & Wambsganss, J., 1990, A&A 237, 42.
- Tanaka, Y., Nandra, K., Fabian, A. C., Inoue, H., Otani, C., Dotani, T., Hayashida, K., Iwasawa, K., Kii, T., Kunieda, H., Makino, F., & Matsuoka, M., 1995, Nature, 375, 659.
- Wambsganss, J. 2001, in Microlensing 2000: A new Era of Microlensing Astrophysics, ed. J.W.Menzies and P.D.Sackett ASP Conf. Series, 239, 351.
- Wambsganss, J., Paczynski, B. 1991, AJ, 102, 86.
- Wandel, A., Peterson, B. M., Malkan, M. A. 1999, ApJ, 526, 579
- Wisotzki, L., Becker, T., Christensen, L., Helms, A., Jahnke, K., Kelz, A., Roth, M. M., Sanchez, S. F. 2003, A&A, 408, 455.
- Wucknitz, O., Wisotzki, L., Lopez, S., Gregg, M.D. 2003, A&A, 405, 445.
- Zakharov, A.F. 1997, Gravitational lenses and microlensing, (Janus-K, Moscow).